Ultrafast electron-lattice thermalization in copper and other noble metal nanoparticles

Denis Mongin[1], Paolo Maioli[1]*, Julien Burgin[2], Pierre Langot[2], Emmanuel Cottancin[1], Sergio D'Addato[3], Bruno Canut[4], Mona Treguer[5], Aurélien Crut[1], Fabrice Vallée[1] and Natalia Del Fatti[1]

[1]Université de Lyon, CNRS, Université Claude Bernard Lyon 1, Institut Lumière Matière, UMR 5306, F-69622 Villeurbanne, France

[2]Université de Bordeaux, CNRS, LOMA, UMR 5798, F-33405 Talence, France

[3]Dipartimento FIM - Università di Modena e Reggio Emilia and CNR NANO, via G. Campi 213/a 41125 Modena Italy

[4]Université de Lyon, Institut des Nanotechnologies de Lyon (UMR5270/CNRS), INSA, Bat. Blaise Pascal, 7 avenue Jean Capelle, F-69621 Villeurbanne cedex, France

[2]Université de Bordeaux, CNRS, ICMCB, UMR 5026, F-33600 Pessac, France

*Corresponding author: paolo.maioli@univ-lyon1.fr

ABSTRACT

Using time-resolved ultrafast pump-probe spectroscopy we investigated the electron-lattice energy transfer in small copper nanospheres with diameters ranging from 3.2 to 23 nm, either embedded in a glass or dispersed in a solvent. Electron-lattice scattering rate is shown to increase with size reduction, in agreement with our previous results obtained on gold and silver nanoparticles in the low excitation regimes. We attribute this effect to the reduction of the screening efficiency of electron-phonon interactions close to the nanoparticle surface. To understand the discrepancy between the results on the electron-lattice scattering in different metals reported in the literature (reduction, no dependence or increase with nanoparticle size), we discuss the experimental conditions required for the accurate determination of electron-lattice energy transfer time from time-resolved investigations in the weak and strong excitation regimes and present power-dependent experiments on gold nanospheres in solution. Our findings are derived from a theoretical analysis based on the two-temperature model predictions and on

a complete modeling of the nanoparticle transient extinction cross-section through the resolution of Boltzmann equation in the presence of hot electrons.

I. INTRODUCTION

The reduction in size of metals down to the nanometric scale and the concomitant appearance of original physical and chemical properties have motivated many experimental and theoretical investigations. The size of metal nanoparticles being intermediate between the one of a macroscopic metal (described by continuous electron energy bands) and an atomic system (discrete energy levels), their physical (e.g. optical, electronic, thermal) response may manifest a transition from a bulk to a molecular behavior. In particular, size reduction can change their ultrafast electron dynamics [1,2], as electron-electron and electron-lattice interactions depend on the wave-functions of conduction and bound electrons, which are modified, as compared to the ones in the bulk, close to the nanoparticle surface. Ultrafast electron dynamics has been largely explored by time-resolved experiments both in monometallic (Ag [2–4], Au [1,2,5–8], Cu [9–11], Pt [5], Sn [12], Ga [13], Na [14]) and bimetallic nanoparticles (AuPt [15], AuAg [16–18], NiAg [18]). In the case of noble metals, silver and gold have been the most investigated, while very few results have been reported on copper nanoparticles, as the higher reactivity of Cu makes it more difficult to synthesize at the nanometric scale and subject to oxidation [19]. Nonetheless, study of its electron dynamics can provide important information on the physical effects which rule electron-electron and electron-lattice interactions (e.g. Coulomb screening mechanisms and their modifications with confinement) in solids and deserve detailed investigations. Previous studies on the internal electron-lattice thermalization in nanometric Cu were made on nanoparticles with diameters from 10 to 30 nm [9–11] and reported either an electron-lattice energy transfer time compatible with the one of bulk copper (about 0.7 ps) [20,21], or an acceleration, attributed to electron coupling to surface vibrational modes [11]. Such an acceleration of electron-lattice energy transfer, inducing a faster electron energy relaxation [2,4], has also been reported in smaller noble metal nanoparticles while other experiments indicated no dependence [7,8,16] or even a decrease of coupling

with size reduction [5]. However, different experimental conditions (as the choice of wavelengths and powers) were used in these optical experiments [22,23].

In this paper, we will first theoretically discuss, in Section II, the choice of these experimental conditions, required for the accurate determination of the electron-lattice energy transfer time through ultrafast time-resolved optical spectroscopy. We will build our analysis both on the simplified two-temperature model (TTM) and on a complete description of the transient nanoparticle extinction cross-section upon ultrafast excitation, and we will support our conclusions with novel experimental investigations on gold nanoparticles in solution. We will then provide, in Section III, results on electron-lattice thermalization in copper nanoparticles.

Ultrafast time-resolved optical spectroscopy is the approach commonly used for investigating the electron energy dynamics of a metal system after an impulsive out-of-equilibrium excitation, giving access to the measurement of its electron-lattice energy transfer rate. This technique consists in measuring the transient changes of the system optical extinction induced by the instantaneous absorption of a femtosecond pump pulse [23–25]. After excitation, hot electrons redistribute their energy by electron-electron interactions (typical timescale of a few hundred femtoseconds in noble metals), leading to internal thermalization of the quasi-free conduction electron gas [24,26]. The energy in excess is transferred to the lattice via electron-lattice energy interactions (picosecond timescale for noble metals), which is the main focus of this work. This, in turn, can be followed by heating-induced nanoparticles mechanical vibrations on a longer timescale [23,27,28], the energy being eventually thermally released to the environment through the particles surface [29–32]. From the optical point of view, the initial electron excitation translates into a fast amplitude modification of the sample extinction (i.e. of the extinction cross-section of the metal nanoparticles), whose decay reflects electron energy loss by electron-lattice energy transfer, with a time constant dependent on the electron-phonon coupling [2,33]. According to the TTM, which is generally used to reproduce the time dependence of electron and lattice temperatures [33,34], electron energy decay time by electron-lattice energy transfer is minimum for a weak excitation and linearly increases with initial electron pump-induced temperature rise, as a consequence of the dependence of the electronic heat

capacity on the temperature. Measurement of electron-lattice thermalization by time-resolved spectroscopy is thus generally made following two different strategies, their comparison and analysis of their validity being the main focus of Section II. The electron energy decay time can be directly measured in the weak excitation regime (initial electron temperature increase of a few hundred degrees). This approach is experimentally challenging as weak excitations translate into small transient optical signals, requiring setups with a high sensitivity. Alternatively, the pump energy-dependent decay time can be measured for different pump pulse energies in experiments with stronger excitations, and the low excitation value subsequently extrapolated. So far, measurements of the electron energy decay time performed in the weak excitation regime have generally shown a decrease of the electron energy loss time constant with size reduction [2,4,12,13], corresponding to a stronger electron-lattice coupling in smaller particles, while experiments in the strong excitation regime reported no dependence [7,8,16,35] or a reduction of coupling [5]. Additionally, while in the weak perturbation regime electron cooling is independent of nanoparticle environment, the latter influences the measured dynamics for a stronger excitation [4,36]. To understand the apparent inconsistency between the results originating from experiments in the weak excitation regime and the ones performed with higher pump power, we will thus include in Section II a detailed study of the TTM predictions and of the more general modeling of transient extinction cross-sections.

Once the main parameters allowing a proper determination of electron-lattice energy transfer rate are elucidated, we will present in Section III a systematic study of the size-dependence of electron-lattice interactions in copper nanospheres in an extended size range (diameters from 3.2 to 23 nm), through ultrafast time-resolved optical spectroscopy, both in the weak and strong excitation regimes. Cu nanoparticles have been synthesized following both physical and chemical methods. This guarantees a variable environments around the nanoparticles and allows to intrinsically attribute the observed size effects to the particles size variations.

II. INVESTIGATING THE ELECTRON-PHONON THERMALIZATION DYNAMICS

A. Optical excitation and two-temperature model (TTM)

Investigating electron-lattice energy exchanges in a material using time-resolved pump-probe spectroscopy requires to properly describe these exchanges and to connect their kinetics to the measured time-dependent optical signals. Assuming the conduction electrons and the lattice vibrations of a metal are independently thermalized, after internal electronic thermalization (see section II.B), at temperature T_e and T_L respectively, TTM predicts that their energy exchanges can simply be modeled by the following rate equations system [33,34,37-40]:

$$\begin{aligned} c_e(T_e)\frac{\partial T_e}{\partial t} &= -g(T_e - T_L) \\ c_L\frac{\partial T_L}{\partial t} &= g(T_e - T_L) \end{aligned} \qquad (1)$$

where $c_e(T_e) = aT_e$ is the temperature-dependent heat capacity per unit volume of the conduction electrons [41], c_L the lattice heat capacity per unit volume and g the electron-phonon coupling constant describing electron-lattice energy exchanges [38,40]. The metallic system is assumed here to be isolated, i.e., the timescale of electron-lattice thermalization is assumed to be much faster than energy transfer to the external environment [42]. The above rate equations are valid for lattice temperatures larger than the Debye temperature and electronic temperature small enough so that only the electrons in the conduction band are perturbed (T_e typically smaller than $T_{e-max} = 3000$ K in Au and Cu and 5000 K in Ag [43]). For larger temperatures, thermal excitation of d-band electrons may lead to modification of the density of electronic states involved in electron-lattice interactions and thus c_e and g [43].

The above system can be solved analytically [20,33], given initial conditions $T_e(t=0) = T_0 + \Delta T_{exc}$ and $T_L(0) = T_0$, T_0 being the initial temperature of the system and ΔT_{exc} the electron temperature increase due to ultrafast electron excitation. In the weak excitation regime ($\Delta T_{exc} < T_0$), the temperature dependence of c_e can be

neglected leading to an exponential decay of the electron excess temperature $\Delta T_e(t)=T_e(t)-T_0$ with time constant $\tau_{e-ph}\approx aT_0/g$ [33,40]. In this approximation, the electron excess energy per unit volume $\Delta u_e(t)=a/2\left[\left(T_0+\Delta T_e(t)\right)^2-T_0^2\right]\approx aT_0\Delta T_e(t)$ is proportional to ΔT_e and thus exhibits the same kinetics as ΔT_e.

In contrast, for stronger excitations ($\Delta T_{exc}>T_0$), the T_e electron temperature decrease is characterized by a longer decay time and a deviation from a purely exponential profile, as a consequence of the linear increase of electron heat capacity with temperature. Solution of TTM shows that, in this strong excitation regime, the times $\tau_{1/e}^{u}$ and $\tau_{1/e}^{T}$ required for the electron excess energy per unit volume, $\Delta u_e(t)$, and temperature, $\Delta T_e(t)$, respectively, to decrease to the $1/e$ fraction of their initial value, are different (solid and dashed lines in Figures 1a and b). Importantly, both $\tau_{1/e}^{u}$ and $\tau_{1/e}^{T}$ linearly increase with initial excitation ΔT_{exc} (Figure 1b), while their dependence on the initial electron excess energy per unit volume, defined as $\Delta u_{exc}=a/2\left[\left(T_0+\Delta T_{exc}\right)^2-T_0^2\right]$ and proportional to pump pulse energy E_{pump}, deviates from linearity (Figure 1a). Comparison of Figures 1a and b directly summarizes the central point of this analysis: experimental extraction of the intrinsic electron-phonon energy transfer time τ_{e-ph}, as the low excitation intercept value of a linear fit of data obtained with stronger perturbations, requires to plot the experimental $\tau_{1/e}^{\mathrm{ex}}$ decay times as a function of ΔT_{exc}, which is to a first approximation proportional to $\sqrt{E_{pump}}$, for $\Delta T_{exc}\gg T_0$, instead of E_{pump}.

B. Optical detection and transient extinction cross-section modeling

The relative transmission variation $\Delta Tr/Tr(\lambda,t)$ of a probe pulse, with wavelength λ, transmitted through a sample (liquid or glass) containing ensembles of nanoparticles, after an initial ($t=0$) excitation by a pump pulse, can be linked to the change of the metal nanoparticles extinction cross-section, $\sigma_{ext}(\lambda,t)$, by $\Delta Tr/Tr(\lambda,t)=-nL\Delta\sigma_{ext}(\lambda,t)$, where n is the nanoparticles density and L the sample

thickness. The time-dependent variation of $\sigma_{ext}(\lambda,t)$ is linked to the metal and environment dynamics through the corresponding dielectric functions ($\varepsilon=\varepsilon_1+i\varepsilon_2$ and ε_m, respectively) changes [24]. Its time-dependent modification can be computed either analytically, for simple geometries [24], or numerically for a generic nanoparticle size and shape, e.g. using finite-element modeling [32]. For weak transmission changes and neglecting the environment heating, $\Delta\sigma_{ext}(\lambda,t)$ simply writes as a function of the wavelength- and time-dependent changes $\Delta\varepsilon_1(\lambda,t)$ and $\Delta\varepsilon_2(\lambda,t)$, using a first order development $\Delta\sigma_{ext}(\lambda,t)=a_1(\lambda)\Delta\varepsilon_1(\lambda,t)+a_2(\lambda)\Delta\varepsilon_2(\lambda,t)$, where $a_{1,2}(\lambda)=\partial\sigma_{ext}/\partial\varepsilon_{1,2}(\lambda)$ are the spectral derivatives of the extinction cross-section. These are strongly spectrally-dispersed around the metal nanoparticle localized Surface Plasmon Resonance (SPR) [24,25,44,45].

As an example, the transient response of 17 nm diameter Au nanoparticles in water is modeled in Figure 2. The sample linear extinction spectrum (inset of Figure 2b, black solid line) and its derivatives $a_{1,2}(\lambda)$ (red dashed and dotted lines) were computed using the multipolar Mie theory. Upon ultrafast excitation by a 50 fs pump pulse (λ_{pump} = 800 nm and ΔT_{exc} = 1 K), the electron occupation number dynamics was obtained by numerical solution of Boltzmann equation, assuming τ_{e-ph} = 1 ps [26,40,46]. A band structure model was subsequently used [47] for calculating the interband transient optical variations dominating the short-time kinetics of the gold dielectric functions $\Delta\varepsilon_{1,2}(\lambda,t)$ [24]. Extinction changes $\Delta\sigma_{ext}(\lambda,t)$ were thus obtained by multiplication of $\Delta\varepsilon_{1,2}(\lambda,t)$ and spectral derivatives $a_{1,2}(\lambda)$ (Figure 2a-b) (temporal and spectral convolution with the 50 fs pulse duration and 15 nm FWHM of the probe pulse were taken into account, see reference [24] for details of all the computations).

In the low perturbation regime, when probing with photon energies lower than all interband transition thresholds ($\lambda >$ 700 nm for Au [24]) and far from SPR, which lies around λ_{SPR} = 520 nm for Au nanospheres in water [44,45], $\Delta\sigma_{ext}(\lambda,t)$ is

dominated by the term $a_1(\lambda)\Delta\varepsilon_1(\lambda,t)$, which is proportional to the electron excess energy per unit volume, $\Delta u_e(t)$ [33,40]. $\Delta\sigma_{ext}(\lambda,t)$ is thus theoretically expected to decay with a characteristic time, $\tau_{1/e}^{th} \approx \tau_{1/e}^{u}$, which varies linearly with ΔT_{exc} (Figure 1) and is independent of λ. This is shown in Figure 2d, where decay times $\tau_{1/e}^{th}$, obtained from the theoretically computed $\Delta\sigma_{ext}(\lambda,t)$ (Figure 2b), are plotted as a function of the λ probe wavelength (squares). Note that, in the strong excitation regime, an additional contribution due to $a_2(\lambda)\Delta\varepsilon_2(\lambda,t)$ can modify the total kinetics of $\Delta\sigma_{ext}(\lambda,t)$, which will be no longer simply related to the electron excess energy, but decays with a time constant that remains linear on ΔT_{exc}.

Conversely, for shorter probe wavelengths ($\lambda < 700$ nm for Au nanospheres), the presence of interband transitions and SPR complicates the analysis of the time-evolution of transient optical signals. At resonance with interband transitions, the transient variations of the extinction cross-section are affected, during electron internal thermalization (a few 100 fs), by the occupation change dynamics of electronic states close to the Fermi level, resulting, at short timescales, in a $\Delta\sigma_{ext}(\lambda,t)$ signal not proportional to $\Delta u_e(t)$ any longer. In addition, the strong dispersion of $a_{1,2}(\lambda)$ spectral derivatives around the SPR translates into a $\Delta\sigma_{ext}(\lambda,t)$ sign change for λ in the vicinity of the SPR [24] (Figure 2a). This is at the origin of $\Delta\sigma_{ext}(\lambda,t)$ complex time-dependences, even for weak perturbations, with decay times smaller than the ones of $\Delta u_e(t)$ and $\Delta T_e(t)$. As shown in Figure 2c, computed $\tau_{1/e}^{th}$ values are scattered when probing around the SPR, potentially leading, for particular probe wavelengths in the 520-535 nm range (hatched area in Figure 2c), to deviations with respect to the τ_{e-ph} = 1 ps electron-lattice energy transfer time. These deviations are concomitant with sign changes of $\Delta\sigma_{ext}(\lambda,t)$ as a function of λ, occurring around 530 nm, as shown in Figure 2c for two different delays (t = 1 and 3 ps, dashed et dotted lines respectively). For probe wavelengths λ distant from the sign change and optimizing $\Delta\sigma_{ext}(\lambda,t)$ amplitude (e.g. 515 and 540 nm,

Figure 2c), $\tau_{1/e}^{th}$ is close to τ_{e-ph}. This is also the case for an infrared probe wavelength (Figure 2d), which is the best choice for obtaining reliable and very weakly scattered $\tau_{1/e}^{th}$ values, directly providing the electron-lattice energy transfer time.

C. Thermalization of gold nanoparticles investigated in different excitation and probe conditions

To experimentally investigate the dependence of the relaxation time, $\tau_{1/e}^{ex}$, of the relative transmission variation $\Delta Tr/Tr(\lambda,t)$ on the experimental conditions and validate extraction of τ_{e-ph}, we measured a series of ultrafast time-resolved pump-probe transmission changes on 17 nm diameter gold nanoparticles in water, both in the weak and strong excitation regimes. For experiments with low excitation, a high repetition rate (80 MHz) home-made infrared Ti:Sa laser oscillator delivering 50 fs pulses with an average power of 1 W was used. Part of the laser output was frequency-doubled by a BBO crystal to generate the blue pump, while the infrared probe power was detected by a photodiode after transmission through the sample. Pump and probe were focused into a 1-mm thick cell containing the nanoparticle solution. Synchronous detection with mechanically chopping at 100 kHz allowed to achieve a noise level $\Delta Tr/Tr$ of the order of 10^{-7}. For experiments with higher pump fluence, the source was replaced by a commercial Ti:Sa amplified system, delivering 800 nm pulses with a 250 kHz repetition rate, 120 fs duration and average power of 1.2 W. An optical parametric amplified (OPA) crystal allowed generation of probe pulses ranging from 480 to 720 nm.

The extinction spectrum of water-immersed gold nanospheres displays a SPR centered aroune 520 nm partially overlapping the interband transitions absorption (Figure 3a) [48,49]. Time-resolved signals were first acquired using the amplified system with pump excitation at 400 nm and probe wavelength at λ = 700, 550 and 525 nm (respectively out of resonance, on one side of the resonance and close to the SPR peak, Figures 3b-d). For each configuration, pump pulse energy E_{pump} was varied from 0.5 to 20 nJ, corresponding to different electron excitation temperatures.

As discussed in the previous section, the fast transmission change at time $t = 0$ for probe wavelength λ = 700 nm and E_{pump} = 0.5 nJ (Figure 3b, black solid

line) corresponds to the pump-induced initial electron excitation [24,46]. Electron energy loss by transfer to the lattice through electron-phonon interactions induces a decay of the time-resolved signal in a few picoseconds. The remaining non-vanishing background is due to thermal excess energy in the nanoparticle, which is transferred to the surrounding environment on a timescale longer than the range investigated here (typically 10 to 100 ps) [29–32]. As expected, exciting with higher power slows down the electron-to-lattice energy transfer (red dashed and blue dotted lines in Figure 3b) [3,7,22,33]. The $\tau_{1/e}^{ex}$ decay can be deduced from the transient optical signal, taking also into account the residual thermal background (Figure 3b, green solid lines).

To plot the measured $\tau_{1/e}^{ex}$ as a function of initial electron temperature increase (Figure 4b), the experimental pump energy E_{pump} must first be converted into the corresponding $\Delta T_{exc} = \sqrt{T_0^2 + 2\Delta u_{exc}/a} - T_0$, where the initial electron excess energy per unit volume is $\Delta u_{exc} = E_{pump} A / (\pi R_{eq}^2 pL)$ (A being the sample linear absorption at the pump wavelength, R_{eq} the pump beam equivalent radius, p the metal volume fraction in the solution and L the thickness of the cell). In the limit of a Gaussian pump beam with waist w_{pump} (radius at $1/e^2$) much larger than the probe beam, $R_{eq} = w_{pump}/\sqrt{2}$.

As expected from the TTM (Figure 1b), the experimental $\tau_{1/e}^{ex}$ dependence is linear on ΔT_{exc} (Figure 4b), the intercept value $\tau_{e-ph} = (0.98 \pm 0.05)$ ps deduced by a linear fit being consistent with the value measured in the weak perturbation regime $\tau_{e-ph} = (0.97 \pm 0.10)$ ps (solid square, Ti:Sa oscillator with λ_{pump}=435 nm, $\lambda = 870$ nm and E_{pump}=0.06 nJ, equivalent to ΔT_{exc} =120 K). This electron-phonon energy transfer time is slightly smaller than the one in bulk gold (~ 1.15 ps) and is consistent with values expected for 17 nm gold nanoparticles, confirming an acceleration of electron-lattice thermalization in gold nanoparticles with size reduction [2]. It should be emphasized that experimental errors in the E_{pump} to ΔT_{exc} conversion (e.g. uncertainties in the determination of R_{eq} or metal volume fraction p) will not prevent

from recovering a linear $\tau_{1/e}^{ex}$ dependence on ΔT_{exc} and will thus have a minor impact on the extrapolated τ_{e-ph} value. Furthermore, considering that ΔT_{exc} is proportional to $\sqrt{\Delta u_{exc}}$ for large enough excitations, and Δu_{exc} is proportional to E_{pump}, $\tau_{1/e}^{ex}$ depends linearly on $\sqrt{E_{pump}}$. Thus, to a first approximation, plotting $\tau_{1/e}^{ex}$ as a function of $\sqrt{E_{pump}}$ will guarantee a correct linear extrapolation of τ_{e-ph}.

As expected theoretically (Figure 1a), $\tau_{1/e}^{ex}$ has a nonlinear dependence on E_{pump} (Figure 4a). In this case, a linear extrapolation can lead to an overestimation of the τ_{e-ph} value, depending on the range of E_{pump} values used for the linear fit. Including $\tau_{1/e}^{ex}$ values corresponding to higher excitation ($T_0+\Delta T_{exc}>T_{e-max}$) can lead to values approximately linear on E_{pump} (inset of Figure 4a), extraction of τ_{e-ph} by a linear fit of $\tau_{1/e}^{ex}$ values against E_{pump} remaining nonetheless unjustified.

On the spectral sideband of the Au nanospheres SPR ($\lambda =$ 550 nm, Figure 3c), time-resolved signals are characterized by a positive transient peak followed by a negative contribution whose relative amplitudes depend on excitation energy (Figure 2c). Strong oscillations due to the mechanical nanoparticle breathing [23,27,28] add-up to the signal, further complicating the determination of the electron energy loss dynamics. All these effects impede extraction of the τ_{e-ph} electron-phonon scattering dynamics when probing in this spectral region.

Although, in the case of probe pulses close to the peak of the SPR ($\lambda =$ 525 nm, Figure 3d), time-resolved signals display a monotonic decay with a dynamics apparently similar to the one with the infrared probe ($\lambda =$ 700 nm, Figure 3b), an exponential function fails to reproduce precisely their decrease, even for low excitation (e.g. green dash-dotted line in Figure 3d, corresponding to a decay time of 0.9 ps, 30% shorter than $\tau_{1/e}^{ex}=$1.2 ps, deduced with $\lambda =$ 700 nm for an equivalent E_{pump}, Figure 4a). This behavior is in agreement with numerical computations (Figure 2a and 2c). As described in the previous section, a choice of probe wavelength too close to the $\Delta Tr/Tr(\lambda,t)$ sign change may prevent from extracting reliable electron-lattice energy transfer time constants.

In conclusion to this section, we detailed the experimental conditions required for a measurement of the electron-lattice energy transfer time τ_{e-ph}. We supported our considerations, based on theoretical models, with experiments performed on Au 17 nm diameter nanoparticles in both weak and strong excitation regimes. The τ_{e-ph} value deduced by a linear fit in experiments with a variable pump energy is reliable and consistent with the value obtained by a direct measurement with pump energy in the weak excitation regime and probe wavelength far from the SPR, provided that (i) linear extrapolation is made on the $\tau_{1/e}^{ex}$ signal plotted against ΔT_{exc} (not E_{pump}), (ii) probe wavelength is tuned on specific spectral regions (either far from SPR, or around the SPR detuned with respect the $\Delta Tr/Tr(\lambda,t)$ sign change wavelength), (iii) investigations are limited to $T_0+\Delta T_{exc}<T_{e-max}$ (3000 K in gold).

III. ELECTRON-LATTICE INTERACTIONS IN COPPER

A. Samples

The electron-phonon energy transfer time has been subsequently determined on Cu nanoparticles with diameters ranging from 23 down to 3.2 nm. To prevent copper oxidation, all the synthesis techniques have in common protection of nanoparticles by embedment in a transparent matrix or immersion in a solvent. To provide different external environments and cover this extended size range, distinct physical and chemical synthesis methods were used.

Cu nanoparticles with diameters 3.2 ± 1.3 (FWHM) nm, 3.8 ± 1.5 nm, 4.8 ± 1.9 nm in an alumina matrix are obtained by Low Energy Cluster Beam Deposition (LECBD) [18,19,50,51]. In this technique, particles are produced by laser vaporization of a copper rod by a pulsed YAG laser, generating atomic plasma in the presence of a continuous flow of helium gas, which is rapidly cooled down by collisions with the inert gas. This induces nucleation and growth of small metal clusters (between 2 and 6 nm in diameter). The cluster/gas mixture expands through a nozzle in a supersonic beam into a high vacuum chamber. The clusters are then codeposited with the transparent matrix on a suprasil glass substrate. Mean nanoparticles size is selected by controlling the inert gas pressure, and size distribution is characterized by transmission electron microscopy (TEM). Metal

density is kept very low to avoid coalescence of the particles after deposition. The glass sample is held at 400 °C [19] during the synthesis to prevent oxidation. To prevent passivation due to ambient exposure, samples are stored under secondary vacuum, their linear absorption spectrum being systematically measured before and after time-resolved experiments to prove no modification. The presence of a SPR peak around 580 nm partially superimposed to interband transitions in the linear extinction spectrum of the 3.2 nm diameter Cu sample (inset in Figure 5a) and x-ray photoelectron spectroscopy (XPS) analysis attests the absence of oxidation [19]. Although nanocrystallinity of these samples has not been determined, its impact on the electron-lattice energy transfer time is expected to be negligible [52].

A 5.0 ± 0.8 nm diameter MgO-embedded copper sample is obtained by a similar technique, using a magnetron-based gas aggregation nanoparticle source [53]. Copper atoms are first evaporated by sputtering with Ar+ ions, then they condensate in clusters inside an aggregation region by cooling after collision with Ar atoms. An electric quadrupole filter selects their mass before co-deposition with magnesium in oxygen atmosphere, resulting in an assembly of the Cu nanoparticles embedded in a MgO matrix [54]. Note that this mass selection stage guarantees a better size selection compared to previous samples, leading to a much smaller size dispersion.

A sample containing 8.0 ± 2.5 nm diameter Cu nanoparticles in a silica glass was obtained from the sol-gel dip-coating technique [55] operating with a constant withdrawal velocity of 8 $cm.min^{-1}$. The sol was composed of a mixture of $Si(OC_2H_5)$(TEOS), $CuNO_3$, H_2O, HNO_3, *n*-propanol ($C_3{}^nH_7OH$) and *i*-butanol ($C_4{}^iH_9OH$). During the dipping procedure, the chamber was maintained under a nitrogen atmosphere so as to lower the humidity ratio below 15%. In order to remove the solvents from the gel, the samples were first dried in air at 100°C for 15 min. After drying, the densification stage was performed by a heat treatment at 500 °C for 15 min in a constant flow of pure and dry oxygen. A layer of copper oxide nanoparticles embedded in silica is thus obtained. Finally the sample is submitted to a reduction treatment carried out at 800 °C for 1 h, using a mixture of 95% N_2 and 5% H_2. This allows obtaining metallic copper nanoparticles embedded in silica, which remain stable in time when making a six layer step dip-coating (no further aging).

Two samples of (17.0 ± 2.5) nm and (23.0 ± 3.5) nm diameter Cu nanoparticles dispersed in water are chemically obtained by gamma rays radiolysis of an initial

solution containing copper sulfates and polymers, following a procedure previously developed for non-noble metals [56]. The irradiated solution presents neutrally charged nanoparticles whose size is tuned by varying the irradiation fluence. An aqueous solution of copper sulfate was irradiated by an ionizing radiation source (1.8 $kGy.h^{-1}$). The irradiated solution contained the metallic precursor ($CuSO_4$) at a concentration of 10^{-3} $mol.L^{-1}$, the stabilizing agent (polyvinyl alcohol (PVA) (2.10^{-3} $mol.L^{-1}$) and an oxidizing radical scavenger (isopropyl alcohol) (10^{-3} $mol.L^{-1}$)). The solutions were degassed and were exposed to gamma radiation to generate the copper nanoparticles. The irradiation was carried out 1 and 2 hours, size distribution being characterized by TEM imaging. The transparent redish solution remained stable even after storage for several months.

B. Results

Electron-lattice energy transfer times in copper nanoparticles were measured by optical time-resolved spectroscopy both in the weak and strong excitation regimes following the experimental conditions discussed in Section II. Normalized transient transmission changes were measured for the 3.2 nm diameter Cu sample with the amplified laser and λ_{pump} =400 nm, λ = 800 nm (probe photon energy far from SPR [19] and lower than all interband transitions thresholds, see the inset of Figure 5a). They highlight an increase of the electron energy decay time for increasing pump pulse energy, as shown in Figure 5a for E_{pump} = 0.6, 1.7 and 4.2 nJ (black solid, red dashed and blue dotted lines respectively), corresponding to ΔT_{exc} = 850, 1670 and 2750 K. This indicates a slowing down of electron-lattice energy transfer with increasing excitation temperature, as in the case of Au nanoparticles (see Section II). As expected, experimental decay time constants $\tau_{1/e}^{\mathrm{ex}}$ extracted from time-resolved signals have a linear dependence on ΔT_{exc} (Figure 5b, red dots), this leading to determination of electron-phonon energy transfer time τ_{e-ph} =(0.29 ± 0.04) ps obtained as the intercept of their linear extrapolation (dashed line) at the origin. As in the case of Au nanoparticles, this value is consistent with the decay time τ_{e-ph} = (0.32 ± 0.04) ps measured in the weak perturbation regime (solid square).

Analogously, $\tau_{1/e}^{ex}$ dependence on pump pulse energy E_{pump} deviates from linearity (inset in Figure 5b), as expected from the TTM.

Electron-phonon energy transfer times τ_{e-ph} were measured for all the other copper samples in the weak perturbation regime (E_{pump} ~0.05 nJ, equivalent to $\Delta T_{exc} \leq$200 K) using the high repetition rate Ti:Sa laser oscillator, with blue pump (λ_{pump} ~ 420 nm) and red probe (λ ~ 840 nm) pulses. τ_{e-ph} dependence on nanoparticle diameters (Figure 6) demonstrates an acceleration of electron-phonon interactions for small particles, compared to the electron-phonon scattering time constant of bulk Cu (620 fs, horizontal dotted line) [20]. No influence of the nanoparticle environment is observed, data being consistent independently of the matrix. The measured decay is thus ascribed to energy loss inside nanoparticles due to intrinsic energy-lattice energy transfer. This reduction with size of electron-lattice energy transfer time was previously measured in other noble metal nanoparticles (Au and Ag), as plotted in the inset of Figure 6 for comparison [2]. In analogy with size effects observed on the internal electron thermalization [1], we qualitatively attribute these effects to the decrease of the screening of the Coulomb electron-ion interaction close to the surface. This is a consequence of the reduction of the density of conduction electrons close to the surfaces (spillout of electron wave-functions) and of the modification of the bound electron localization in the nanoparticle core [2,57], these effects being more important on smaller particles with higher surface-to-volume ratio. While the first time-resolved optical experiments on copper nanoparticles have not specifically addressed the size-dependence of electron-lattice scattering, their measured electron relaxation times [9,10] are in agreement with an optical excitation in the strong perturbation regime. The acceleration of electron-lattice interactions with size reduction previously reported for two samples of copper nanoparticles in colloidal solution, with diameters of 12 and 30 nm [11] is qualitatively consistent with the present findings. However, the electron-lattice energy transfer times experimentally measured (0.37 and 0.51 ps for the 12 and 30 nm sample respectively) are approximately 25% smaller than the ones reported in our work, which can be explained by the additional presence of surface imperfections as mentioned by the authors.

The difference in the absolute values of electron relaxation times and their size-dependencies for Cu, Au and Ag (Figure 6, inset) could be ascribed to different electronic and dielectric properties (electron density, electron effective mass and static interband dielectric constant), these parameters ruling the screening efficiency of conduction and bound electrons [1,2,46]. However, this model, based on a bulk approach modified by surface effects, allows a quantitative reproduction of the size-dependent acceleration of internal electron thermalization by electron-electron scattering [1], but only a qualitatively description of electron-phonon time-evolution in Au and Ag [2,57] and Cu. A more complete and quantitative analysis of the electron-lattice interaction in noble metal nanoparticles, requiring quantum treatment of both electronic and phononic energy states and of their coupling, is still missing and is out of the scope of this study.

IV. CONCLUSIONS

In conclusion, we have investigated electron-phonon thermalization on noble metal nanoparticles by comparing experiments in the weak and strong perturbation regimes, and discussed experimental choices and analysis conditions required for carefully extracting electron-lattice energy transfer time constants. Using this analysis, we have performed a systematic study of electron-lattice thermalization on Cu nanoparticles, which proves an acceleration of electron-phonon interactions with reduction in size, similar to the behavior observed in Au and Ag. This effect is independent of nanoparticle environment (solid or liquid) and is qualitatively attributed to a modification of the screening of Coulomb electron-ion interactions close to the surface, when reducing the metal nanoparticle size. Extension of these measurements to electron thermalization in small clusters (< 2 nm size) is currently an active field of investigation, providing useful information to explain the transition from small-solid to molecular-like behavior in electronic interactions at the nanoscale.

REFERENCES

[1] Voisin C, Christofilos D, Del Fatti N, Vallée F, Prével B, Cottancin E, Lermé J, Pellarin M and Broyer M 2000 Size-Dependent Electron-Electron Interactions in Metal Nanoparticles *Phys. Rev. Lett.* **85** 2200–3

[2] Arbouet A, Voisin C, Christofilos D, Langot P, Del Fatti N, Vallée F, Lermé J, Celep G, Cottancin E, Gaudry M, Pellarin M, Broyer M, Maillard M, Pileni M P and Treguer M 2003 Electron-Phonon Scattering in Metal Clusters *Phys. Rev. Lett.* **90** 177401

[3] Hodak J H, Martini I and Hartland G V. 1998 Spectroscopy and Dynamics of Nanometer-Sized Noble Metal Particles *J. Phys. Chem. B* **102** 6958–67

[4] Halté V, Bigot J-Y, Palpant B, Broyer M, Prével B and Pérez A 1999 Size dependence of the energy relaxation in silver nanoparticles embedded in dielectric matrices *Appl. Phys. Lett.* **75** 3799

[5] Smith B A, Zhang J Z, Giebel U and Schmid G 1997 Direct probe of size-dependent electronic relaxation in single-sized Au and nearly monodisperse Pt colloidal nano-particles *Chem. Phys. Lett.* **270** 139–44

[6] Link S, Burda C, Mohamed M, Nikoobakht B and El-Sayed M A 2000 Femtosecond transient-absorption dynamics of colloidal gold nanorods: Shape independence of the electron-phonon relaxation time *Phys. Rev. B* **61** 6086–90

[7] Hodak J H, Martini I and Hartland G V. 1998 Ultrafast study of electron–phonon coupling in colloidal gold particles *Chem. Phys. Lett.* **284** 135–41

[8] Hodak J H, Henglein A and Hartland G V. 2000 Electron-phonon coupling dynamics in very small (between 2 and 8 nm diameter) Au nanoparticles *J. Chem. Phys.* **112** 5942

[9] Tokizaki T, Nakamura A, Kaneko S, Uchida K, Omi S, Tanji H and Asahara Y 1994 Subpicosecond time response of third-order optical nonlinearity of small copper particles in glass *Appl. Phys. Lett.* **65** 941–3

[10] Bigot J-Y, Merle J, Cregut O and Daunois A 1995 Electron Dynamics in Copper Metallic Nanoparticles Probed with Femtosecond Optical Pulses *Phys. Rev. Lett.* **75** 4702–5

[11] Darugar Q, Qian W, El-Sayed M A and Pileni M-P 2006 Size-dependent ultrafast electronic energy relaxation and enhanced fluorescence of copper

nanoparticles. *J. Phys. Chem. B* **110** 143–9

[12] Stella A, Nisoli M, De Silvestri S and Svelto O 1996 Size effects in the ultrafast electronic dynamics of metallic tin nanoparticles *Phys. Rev. B* **53** 15497–500

[13] Nisoli M, Stagira S, De Silvestri S, Stella A, Tognini P, Cheyssac P and Kofman R 1997 Ultrafast Electronic Dynamics in Solid and Liquid Gallium Nanoparticles *Phys. Rev. Lett.* **78** 3575–8

[14] Maier M, Wrigge G, Hoffmann M A, Didier P and Issendorff B V. 2006 Observation of Electron Gas Cooling in Free Sodium Clusters *Phys. Rev. Lett.* **96** 117405

[15] Hodak J H, Henglein A and Hartland G V. 2001 Tuning the spectral and temporal response in PtAu core–shell nanoparticles *J. Chem. Phys.* **114** 2760–5

[16] Link S, Burda C, Wang Z L and El-Sayed M A 1999 Electron dynamics in gold and gold–silver alloy nanoparticles: The influence of a nonequilibrium electron distribution and the size dependence of the electron–phonon relaxation *J. Chem. Phys.* **111** 1255

[17] Hodak J H, Henglein A and Hartland G V. 2000 Photophysics of Nanometer Sized Metal Particles: Electron−Phonon Coupling and Coherent Excitation of Breathing Vibrational Modes *J. Phys. Chem. B* **104** 9954–65

[18] Broyer M, Cottancin E, Lermé J, Pellarin M, Del Fatti N, Vallée F, Burgin J, Guillon C and Langot P 2008 Optical properties and relaxation processes at femtosecond scale of bimetallic clusters *Faraday Discuss.* **138** 137–45

[19] Celep G, Cottancin E, Lermé J, Pellarin M, Arnaud L, Huntzinger J, Vialle J-L, Broyer M, Palpant B, Boisron O and Mélinon P 2004 Optical properties of copper clusters embedded in alumina: An experimental and theoretical study of size dependence *Phys. Rev. B* **70** 165409

[20] Brorson S D, Kazeroonian A, Moodera J S, Face D W, Cheng T K, Ippen E P, Dresselhaus M S and Dresselhaus G 1990 Femtosecond room-temperature measurement of the electron-phonon coupling constant y in metallic superconductors *Phys. Rev. Lett.* **64** 2172–5

[21] Elsayed-Ali H, Norris T, Pessot M and Mourou G 1987 Time-resolved observation of electron-phonon relaxation in copper *Phys. Rev. Lett.* **58** 1212–5

[22] Hartland G V. 2004 Measurements of the material properties of metal nanoparticles by time-resolved spectroscopy *Phys. Chem. Chem. Phys.* **6** 5263

[23] Hartland G V. 2011 Optical studies of dynamics in noble metal nanostructures *Chem. Rev.* **111** 3858–87

[24] Stoll T, Maioli P, Crut A, Del Fatti N and Vallée F 2014 Advances in femto-nano-optics: ultrafast nonlinearity of metal nanoparticles *Eur. Phys. J. B* **87** 260

[25] Crut A, Maioli P, Vallée F and Del Fatti N 2017 Linear and ultrafast nonlinear plasmonics of single nano-objects *J. Phys. Condens. Matter* **29** 123002

[26] Voisin C, Del Fatti N, Christofilos D and Vallée F 2001 Ultrafast Electron Dynamics and Optical Nonlinearities in Metal Nanoparticles *J. Phys. Chem. B* **105** 2264–80

[27] Crut A, Maioli P, Del Fatti N and Vallée F 2015 Acoustic vibrations of metal nano-objects: Time-domain investigations *Phys. Rep.* **549** 1–43

[28] Maioli P, Stoll T, Sauceda H E, Valencia I, Demessence A, Bertorelle F, Crut A, Vallée F, Garzón I L, Cerullo G and Del Fatti N 2018 Mechanical Vibrations of Atomically Defined Metal Clusters: From Nano- to Molecular-Size Oscillators *Nano Lett.* **18** 6842–9

[29] Cahill D G, Braun P V., Chen G, Clarke D R, Fan S, Goodson K E, Keblinski P, King W P, Mahan G D, Majumdar A, Maris H J, Phillpot S R, Pop E and Shi L 2014 Nanoscale thermal transport. II. 2003–2012 *Appl. Phys. Rev.* **1** 011305

[30] Juvé V, Scardamaglia M, Maioli P, Crut A, Merabia S, Joly L, Del Fatti N and Vallée F 2009 Cooling Dynamics and Thermal Interface Resistance of Glass-Embedded Metal Nanoparticles *Phys. Rev. B* **80** 195406

[31] Stoll T, Maioli P, Crut A, Rodal-Cedeira S, Pastoriza-Santos I, Vallée F and Del Fatti N 2015 Time-Resolved Investigations of the Cooling Dynamics of Metal Nanoparticles: Impact of Environment *J. Phys. Chem. C* **119** 12757–12764

[32] Gandolfi M, Crut A, Medeghini F, Stoll T, Maioli P, Vallée F, Banfi F and Del Fatti N 2018 Ultrafast Thermo-Optical Dynamics of Plasmonic Nanoparticles *J. Phys. Chem. C* **122** 8655–66

[33] Del Fatti N, Arbouet A and Vallée F 2006 Femtosecond Optical Investigation of Electron–Lattice Interactions in an Ensemble and a Single Metal Nanoparticle *Appl. Phys. B* **84** 175–81

[34] Kaganov M I, Lifshitz I M and Tanatarov L V 1957 Relaxation between electrons and the crystalline lattice *Sov. Phys. JETP* **4** 173

[35] Link S, El-Sayed M A, Schaaff T G and RL 2002 Transition from nanoparticle to molecular behavior: a femtosecond transient absorption study of a size-selected 28 atom gold cluster *Chem. Phys. Lett.* **356** 240–6

[36] Mohamed M B, Ahmadi T S, Link S, Braun M and El-Sayed M A 2001 Hot electron and phonon dynamics of gold nanoparticles embedded in a gel matrix *Chem. Phys. Lett.* **343** 55–63

[37] Anisimov S I, Kapeliovich B L and Perel'man T L 1974 Electron emission from metal surfaces exposed to ultrashort laser pulses *Sov. Phys. JETP* **39** 375–7

[38] Allen P B 1987 Theory of thermal relaxation of electrons in metals *Phys. Rev. Lett.* **59** 1460–3

[39] Groeneveld R, Sprik R and Lagendijk A 1995 Femtosecond spectroscopy of electron-electron and electron-phonon energy relaxation in Ag and Au. *Phys. Rev. B* **51** 11433–45

[40] Del Fatti N, Voisin C, Achermann M, Tzortzakis S, Christofilos D and Vallée F 2000 Nonequilibrium electron dynamics in noble metals *Phys. Rev. B* **61** 16956–66

[41] Ashcroft N W and Mermin N D 1976 *Solid State Physics* (New York: Holt, Rinehart and Winston)

[42] Grua P, Morreeuw J P, Bercegol H, Jonusauskas G and Vallée F 2003 Electron kinetics and emission for metal nanoparticles exposed to intense laser pulses *Phys. Rev. B* **68** 035424

[43] Lin Z, Zhigilei L and Celli V 2008 Electron-phonon coupling and electron heat capacity of metals under conditions of strong electron-phonon nonequilibrium *Phys. Rev. B* **77** 1–17

[44] Kelly K L, Coronado E, Zhao L L and Schatz G C 2003 The optical properties of metal nanoparticles: the influence of size, shape, and dielectric environment *J. Phys. Chem. B* **107** 668–77

[45] Crut A, Maioli P, Del Fatti N and Vallée F 2014 Optical absorption and scattering spectroscopies of single nano-objects. *Chem. Soc. Rev.* **43** 3921–56

[46] Voisin C, Christofilos D, Loukakos P, Del Fatti N, Vallée F, Lermé J, Gaudry M, Cottancin E, Pellarin M and Broyer M 2004 Ultrafast Electron-Electron Scattering and Energy Exchanges in Noble-Metal Nanoparticles *Phys. Rev. B* **69** 195416

[47] Rosei R 1974 Temperature modulation of the optical transitions involving the Fermi surface in Ag: Theory *Phys. Rev. B* **10** 474–83

[48] Myroshnychenko V, Rodríguez-Fernández J, Pastoriza-Santos I, Funston A M, Novo C, Mulvaney P, Liz-Marzán L M and García de Abajo F J 2008 Modelling the optical response of gold nanoparticles. *Chem. Soc. Rev.* **37** 1792–805

[49] Liz-Marzán L M 2006 Tailoring surface plasmons through the morphology and assembly of metal nanoparticles. *Langmuir* **22** 32–41

[50] Alayan R, Arnaud L, Bourgey A, Broyer M, Cottancin E, Huntzinger J R, Lermé J, Vialle J-L, Pellarin M and Guiraud G 2004 Application of a static quadrupole deviator to the deposition of size-selected cluster ions from a laser vaporization source *Rev. Sci. Instrum.* **75** 2461–70

[51] Perez A, Melinon P, Dupuis V, Bardotti L, Masenelli B, Tournus F, Prével B, Tuaillon-Combes J, Bernstein E, Tamion A, Blanc N, Tainoff D, Boisron O, Guiraud G, Broyer M, Pellarin M, Del Fatti N, Vallée F, Cottancin E, Lermé J, Vialle J-L, Bonnet C, Maioli P, Crut A, Clavier C, Rousset J L and Morfin F 2010 Functional nanostructures from clusters *Int. J. Nanotechnol.* **7** 523–74

[52] Goubet N, Tempra I, Yang J, Soavi G, Polli D, Cerullo G and Pileni M P 2015 Size and nanocrystallinity controlled gold nanocrystals: synthesis, electronic and mechanical properties *Nanoscale* **7** 3237–46

[53] D'Addato S and Spadaro M C 2018 Low pressure bottom-up synthesis of metal@oxide and oxide nanoparticles: control of structure and functional properties *Phys. Scr.* **93** 033001

[54] D'Addato S, Grillo V, Altieri S, Frabboni S, Rossi F and Valeri S 2011 Assembly and Fine Analysis of Ni/MgO Core/Shell Nanoparticles *J. Phys. Chem. C* **115** 14044–9

[55] De G, Gusso M, Tapfer L, Catalano M, Gonella F, Mattei G, Mazzoldi P and Battaglin G 1996 Annealing behavior of silver, copper, and silver–copper nanoclusters in a silica matrix synthesized by the sol-gel technique *J. Appl. Phys.* **80** 6734

[56] Benoit R, Sabougi M L and Tréguer-Delapierre M 2003 Effect of radiation dose on the size of bismuth particles produced by radiolysis *Eur. Phys. J. D* **24** 123–5

[57] Lermé J, Celep G, Broyer M, Cottancin E, Pellarin M, Arbouet A, Christofilos

D, Guillon C, Langot P, Del Fatti N and Vallée F 2005 Effects of confinement on the electron and lattice dynamics in metal nanoparticles *Eur. Phys. J. D* **34** 199–204

[58] Weaver J H and Frederikse H P R 1977 *CRC Handbook of Chemistry and Physics* (CRC Press)

[59] Bohren C F and Huffman D R 1983 *Absorption and Scattering of Light by Small Particles* (New York: Wiley)

[60] Johnson P B and Christy R W 1972 Optical Constants of the Noble Metals *Phys. Rev. B* **6** 4370–9

[61] Baida H, Billaud P, Marhaba S, Christofilos D, Cottancin E, Crut A, Lermé J, Maioli P, Pellarin M, Broyer M, Del Fatti N, Vallée F, Sánchez-Iglesias A, Pastoriza-Santos I and Liz-Marzán L M 2009 Quantitative determination of the size dependence of surface plasmon resonance damping in single Ag@SiO(2) nanoparticles. *Nano Lett.* **9** 3463–9

[62] Juvé V, Cardinal M F, Lombardi A, Crut A, Maioli P, Pérez-Juste J, Liz-Marzán L M, Del Fatti N and Vallée F 2013 Size-dependent surface plasmon resonance broadening in nonspherical nanoparticles: single gold nanorods. *Nano Lett.* **13** 2234–40

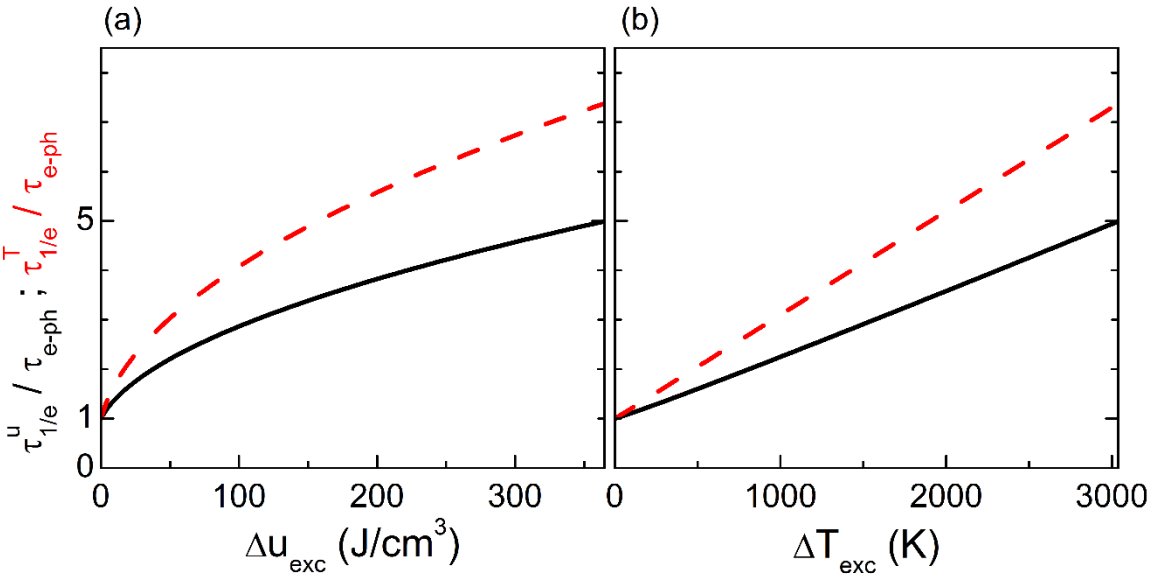

Figure 1. Decay time constants, $\tau^{u}_{1/e}$ and $\tau^{T}_{1/e}$, of the electron excess energy per unit volume, $\Delta u_e(t)$, and electron temperature increase, $\Delta T_e(t)$, (solid and dashed line) computed in gold, after an impulsive out-of-equilibrium excitation, as a function of initial electron excess energy per unit volume Δu_{exc} (a) and electron excitation temperature ΔT_{exc} (b), normalized to their low excitation value τ_{e-ph}. They are obtained from the two-temperature model (equation 1), with $a = 65\ \mathrm{J/(m^3\ K^2)}$, $c_L = 2.49 \cdot 10^6\ \mathrm{J/(m^3\ K)}$ and $g = 1.7 \cdot 10^{16}\ \mathrm{J/(m^3\ K \cdot\ s)}$ [33,58].

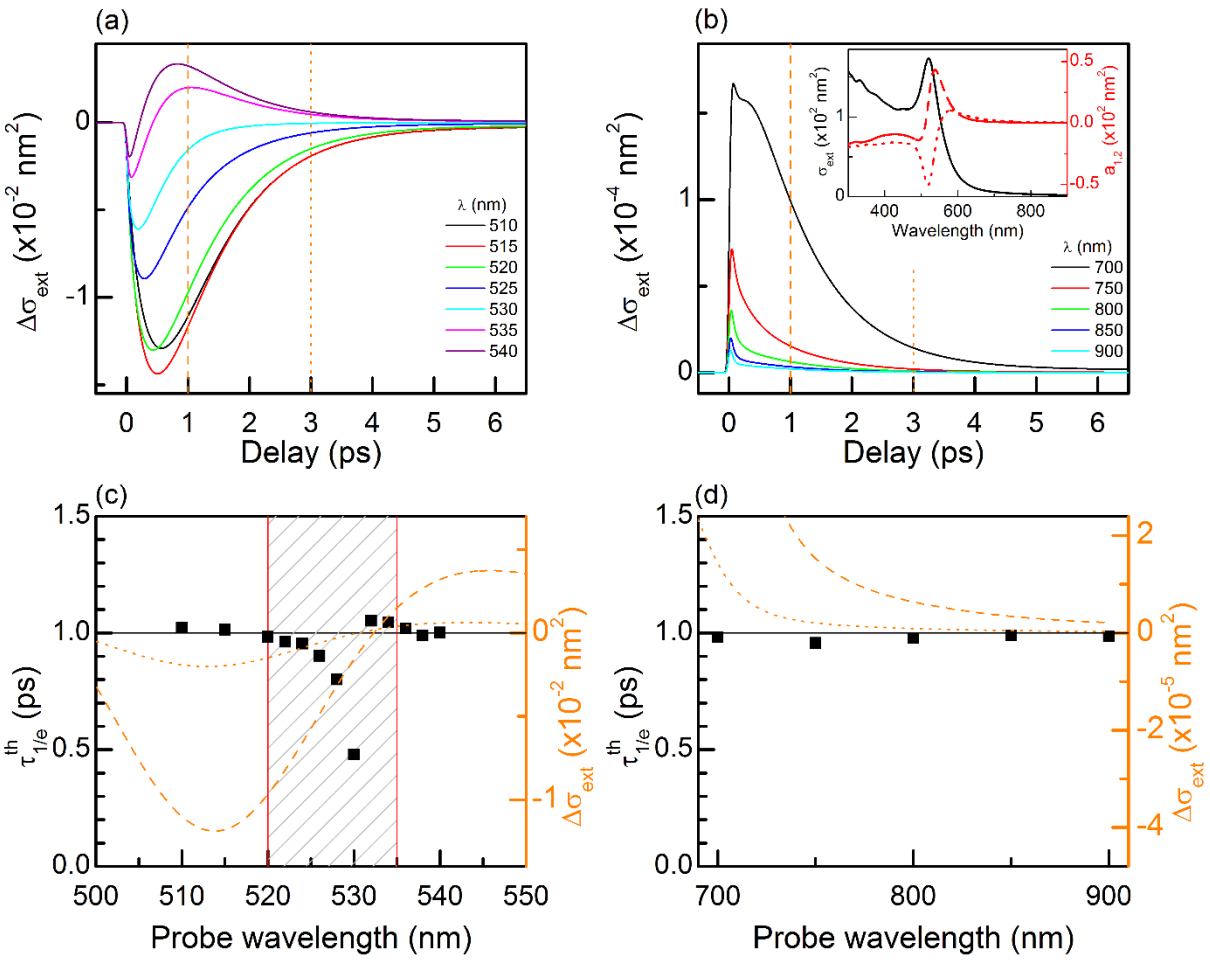

Figure 2. (a, b) Computation of the time-evolution of extinction cross-section variation $\Delta\sigma_{ext}(\lambda,t)$ of a 17 nm diameter Au nanosphere for probe wavelengths λ indicated inside the graph (ΔT_{exc}= 1 K, 50 fs pump pulse at λ_{pump} = 800 nm, 50 fs probe pulse with 15 nm FWHM spectral width, τ_{e-ph} = 1 ps). Inset in panel b shows the linear extinction cross-section of a 17 nm diameter Au nanosphere in water (black solid line, left axis) computed by Mie multipolar theory [59] with an effective environment refractive index n=1.26, Johnson and Christy dielectric functions for bulk gold [60] and electron surface-scattering factor g=0.8 [61,62], together with its $a_1(\lambda)$ and $a_2(\lambda)$ derivatives (right axis, red dashed and dotted lines respectively). The linear spectrum is a fit of the experimental extinction spectrum of Figure 3a. (c-d) Decay time $\tau_{1/e}^{th}$ as a function of the probe wavelength obtained by a monoexponential fit of the computed $\Delta\sigma_{ext}(\lambda,t)$ decay (squares, left axis).

$\Delta\sigma_{ext}(\lambda,t)$ at t=1 and 3 ps after excitation are plotted in the same graph (orange dashed and dotted lines respectively, right axis). These delays are indicated in panel a-b with vertical dashed and dotted lines. The hatched area in panel c indicates the range of probe wavelengths inappropriate for the measurement of electron-phonon energy transfer time (predicted decay times $\tau_{1/e}^{th}$ shorter than τ_{e-ph} = 1 ps).

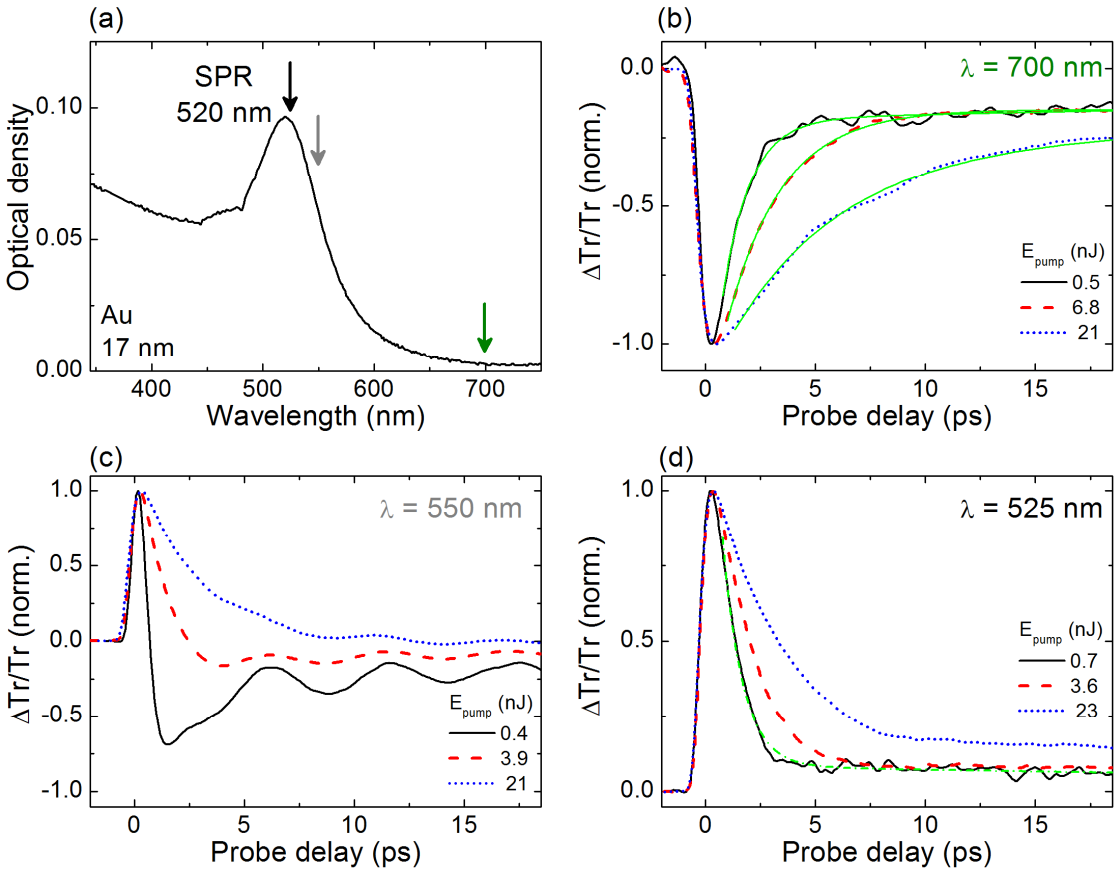

Figure 3. (a) Extinction spectrum of 17 nm diameter gold nanospheres in water. (b-d) Normalized transient transmission changes $\Delta Tr / Tr(\lambda, t)$, measured used different excitation energies (black solid, red dashed and blue dotted lines) with pump wavelength λ_{pump} = 400 nm and probe wavelength tuned to λ = 700 nm (b), 550 nm (c) and 525 nm (d). Green solid lines in (b) represent the fits of the three signals with an exponential decaying function and a residual backgound. Pump pulse energies E_{pump} are indicated inside the graphs. Vertical arrows in (a) indicate the positions of the probe wavelengths on the linear extinction spectrum. Green dash-dotted line in (d) represents an exponential fit of the time-resolved signal at E_{pump}= 0.7 nJ (solid line).

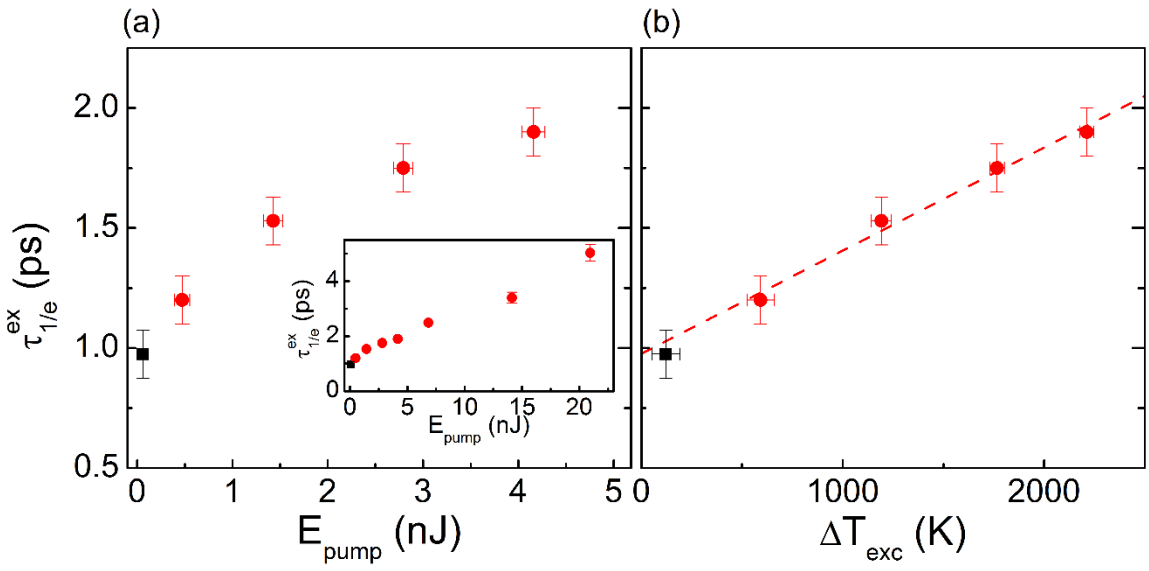

Figure 4. Decay time constants $\tau_{1/e}^{ex}$ deduced from experiments in 17 nm diameter gold nanoparticles in water with pump wavelength λ_{pump}= 400 nm, probe wavelength λ = 700 nm and variable excitation energy (red dots), and λ_{pump}= 435 nm and λ = 870 nm in the weak perturbation regime (black square), plotted as a function of pump pulse energy E_{pump} (a) and electron excitation temperature ΔT_{exc} (b). Dashed line in (b) is a linear fit of $\tau_{1/e}^{ex}$ values obtained with stronger perturbations (red dots). Inset in (a) shows experimental $\tau_{1/e}^{ex}$ on a larger E_{pump} range.

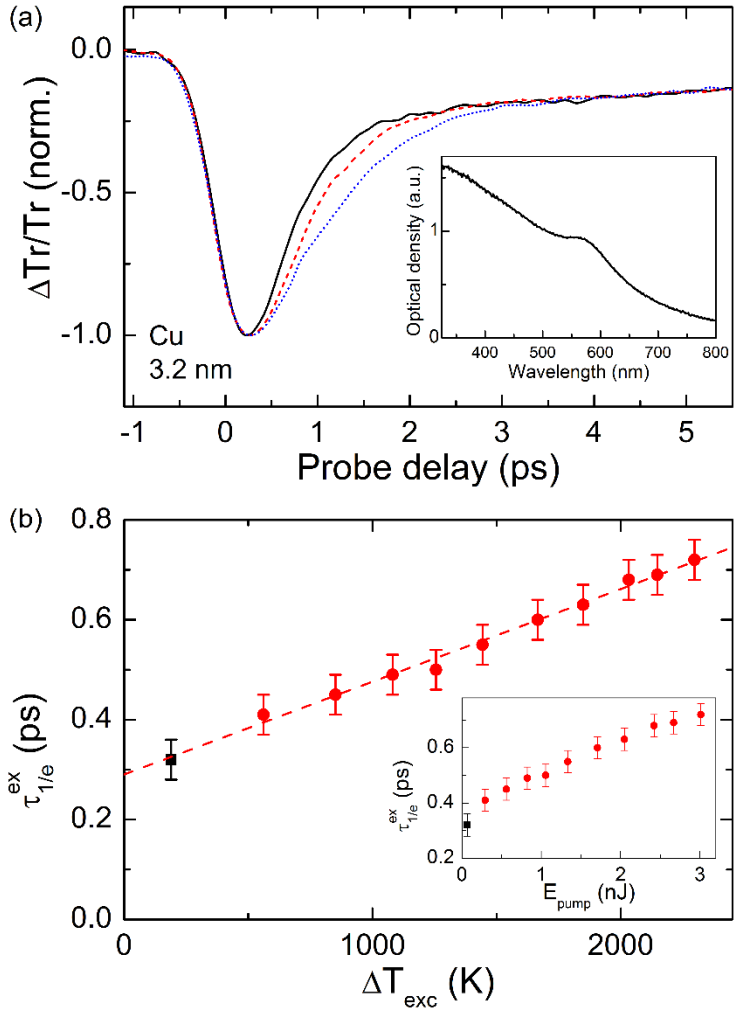

Figure 5. (a) Normalized transient transmission changes, $\Delta Tr/Tr(\lambda,t)$, on 3.2 nm diameter Cu nanospheres embedded in alumina, measured with amplified Ti:Sa laser with a repetition rate of 250 kHz, λ_{pump}= 400 nm and probe wavelength λ = 800 nm, and excitation energies corresponding to ΔT_{exc}= 850 K (black solid line, corresponding to pump pulse energy E_{pump} = 0.6 nJ), 1670 K (red dashed line, E_{pump} = 1.7 nJ) and 2750 K (blue dotted line, E_{pump} =4.2 nJ). Inset shows the linear extinction spectrum of the sample. (b) Experimental decay time constants $\tau_{1/e}^{ex}$ extracted from time-resolved signals in the strong excitation regime (red dots) and their linear fit (dashed line), and for a weak pump excitation (black square, measured with λ_{pump}= 420 nm and λ = 840 nm, E_{pump} = 0.06 nJ), plotted as a function of electron excitation temperature ΔT_{exc} (main graph) and pump pulse energy E_{pump} (inset).

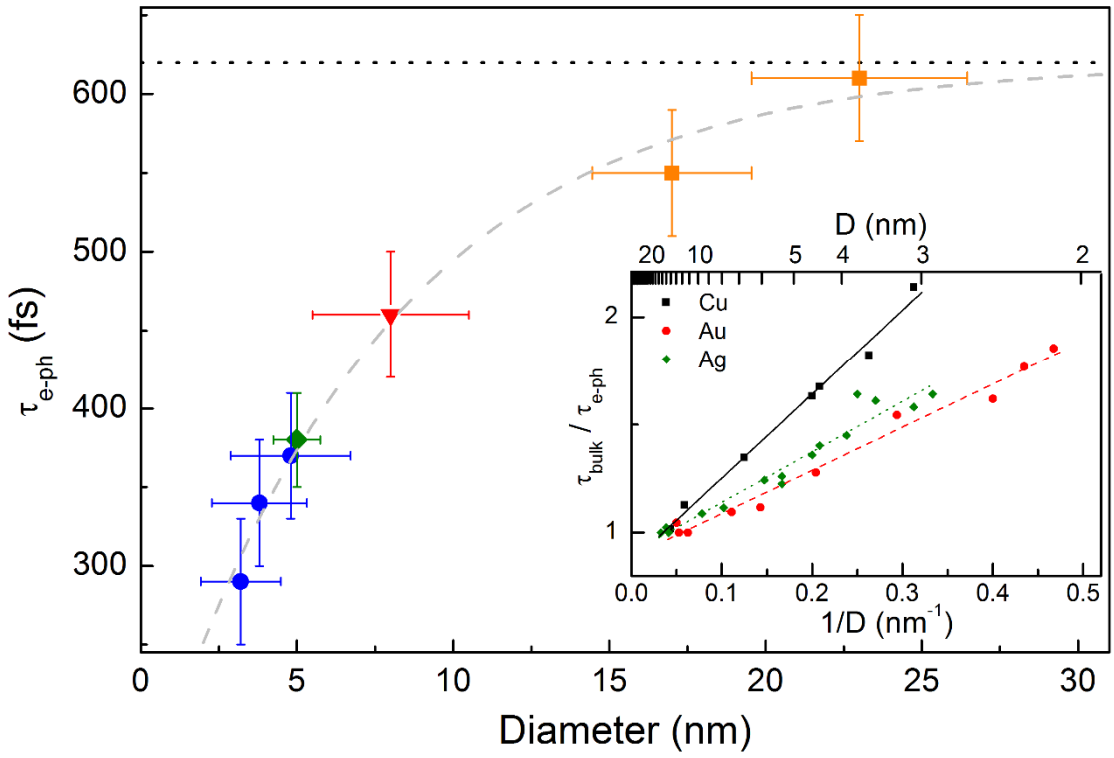

Figure 6. Experimental electron-lattice energy transfer time constants, τ_{e-ph}, of Cu nanoparticles as a function of their diameter. Samples are obtained by Low Energy Cluster Beam Deposition in alumina (blue dots), magnetron sputtering deposition in magnesia (green diamond), sol-gel dip-coating in silica (red triangle) and chemical radiolysis in water (orange squares). Horizontal dotted line represents τ_{e-ph} value for bulk Cu. Grey dashed line is a guide for the eyes. Inset shows experimental electron-lattice transfer rates, $1/\tau_{e-ph}$, normalized to the one of the bulk, as a function of the inverse diameter, obtained for Cu (squares, this work), Au (dots) and Ag (diamonds) [2], with qualitative linear fits.